Applied Surface Science 292 (2014) 843–851

Contents lists available at ScienceDirect

Applied Surface Science

journal homepage: www.elsevier.com/locate/apsusc

Drug release from porous silicon for stable neural interface

Tao Sun [a,*], Wei Mong Tsang [a], Woo-Tae Park [a,b]

[a] Institute of Microelectronics, Agency for Science, Technology and Research (A*STAR), Singapore
[b] Department of Mechanical and Automotive Engineering, Seoul National University of Science and Technology, Seoul, Republic of Korea

ARTICLE INFO

Article history:
Received 18 August 2013
Received in revised form 5 December 2013
Accepted 10 December 2013
Available online 17 December 2013

Keywords:
Neural interface
Drug release
Porous silicon
Dexamethasone
Primary astrocyte

ABSTRACT

70 μm-thick porous Si (PSi) layer with the pore size of 11.1 ± 7.6 nm was formed on an 8-in. Si wafer via an anodization process for the microfabrication of a microelectrode to record neural signals. To reduce host tissue responses to the microelectrode and achieve a stable neural interface, water-soluble dexamethesone (Dex) was loaded into the PSi via incubation with the drug solution overnight. After the drug loading process, the pore size of PSi reduced to 4.7 ± 2.6 nm on the basis of scanning electron microscopic (SEM) images, while its wettability was remarkably enhanced. Fluorescence images demonstrated that Dex was loaded into the porous structure of the PSi. Degradation rate of the PSi was investigated by incubation in distilled water for 21 days. Moreover, the drug release profile of the Dex-loaded PSi was a combination of an initial burst release and subsequent sustained release. To evaluate cellular responses to the drug release from the PSi, primary astrocytes were seeded on the surface of samples. After 2 days of culture, the Dex-loaded PSi could not only moderately prevent astrocyte adhesion in comparison with Si, but also more effectively suppress the activation of primary astrocytes than unloaded PSi due to the drug release. Therefore, it might be an effective method to reduce host tissue responses and stabilize the quality of the recorded neural signal by means of loading drugs into the PSi component of the microelectrode.

1. Introduction

Simultaneously recorded neural signals from brain can be translated into command signals to drive prosthetic limbs or computer displays, and realize the intended motions of the patient for the purpose of restoring lost motor functions [1,2]. In contrast to non-invasive approaches to record brain activities, such as electroencephalography (EEG), neural microelectrode implanted into cortical tissues is capable of recording high-precise neural signals to control the robotic devices with multiple degrees of freedom. Although the emergence of the fully implantable neural microelectrodes rekindles the hope of patients suffering from paralyzation, one of the major technological barriers for their widespread clinical applications is to establish a stable neural interface between the signal recording sites (microelectrodes) and delicate neural tissues. The unstable neural interface eventually gives rise to the failure of neural prostheses due to the loss of neural signals. An earlier study by Williams et al. showed the number of microelectrodes recording signals from cats dropped to 5 of 8 after 15 weeks implantation [3]. A later clinical study for a tetraplegic human with the aim of restoring lost motor functions via a pilot neuromotor prosthesis found abrupt signal loss at most electrodes after 11 months implantation [4]. More recently, it was reported that useful signals were obtained each day more than 2.7 years after a 4 mm × 4 mm array of 100 microelectrodes was implanted into the motor cortex of a human with longstanding tetraplegia subsequent to a brainstem stroke [5]. However, the longevity of current neural microelectrodes still does not meet the market requirement, and the neural prostheses should remain functional for a long term over the patients' lifetime.

The main failure modes of microelectrodes include the fibrous tissue encapsulation by gliosis, the loss of neurons surrounding the electrodes, and post-implantation injury caused by brain micromotion and the mismatch in mechanical properties between cortical tissues (~10 kPa) and microelectrodes (~170 GPa for Si) [6–8]. Due to its nano-featured surface, porous Si (PSi) has been considered as a promising electrode material in a nerve repair setting [9]. Moreover, Misra et al. reported that microelectrodes were microfabricated from PSi substrates with ceramic insulation as part of their ongoing work [10]. However, degradability and drug-loading capability of PSi have not been taken advantage of in the design of neural microelectrode to create a stable neural interface and elongate the lifetime of the microelectrode. We are proposing a novel PSi-polymer hybrid microelectrode consisting of a PSi backbone, parylene insulating layers and gold recording sites. The PSi backbone has enough strength with the function of penetrating into cortical tissues. After degradation of the PSi backbone, the remaining thin parylene insulating layers (5–10 μm) maintains the flexibility to minimize post-implantation injury. Moreover, the PSi

* Corresponding author. Tel.: +65 6770 5468; fax: +65 6774 5754.
E-mail addresses: taosun@hotmail.com.hk, sunt@ime.a-star.edu.sg (T. Sun).

0169-4332/$ – see front matter © 2013 Elsevier B.V. All rights reserved.
http://dx.doi.org/10.1016/j.apsusc.2013.12.060

backbone can serve as the reservoir to deliver drugs for reduced host tissue responses. In our previous studies, the PSi backbone has been successfully developed via standard microelectromechanical systems (MEMS) technologies [11].

Dexamethesone (Dex) is one of popular anti-inflammatory drugs to minimize host tissue responses caused by the implantation of neural prostheses. Spataro et al. suggested that subcutaneous injection of Dex for 6 days remarkably attenuated astrocytic responses around inserted neural prosthetic devices [12]. Zhong and Bellamkonda coated Dex-nitrocellulose layers on microelectrodes via evaporation of the mixture of Dex and nitrocellulose solution, and found that the Dex-nitrocellulose coating could effectively reduce the loss of neurons surrounding the coated neural electrodes and suppress the inflammatory responses [13]. Additionally, sustained and controlled release of Dex from polymeric nanoparticles embedded in alginate hydrogel coating was investigated by Kim and Martin [14]. After 2-week implantation the impedance of the electrodes loaded with Dex almost maintained stable, and the reduced fibrous tissue encapsulation was thought to be responsible for the relatively stable impedance over time. Hence, in this research Dex was chosen to load into the PSi owing to its well-established model.

As a fundamental study to develop the PSi-polymer hybrid microelectrode, PSi was prepared via an anodization process in this study, and then Dex was loaded into the PSi to investigate the drug release profile. The surface characteristics, wettability, degradability, drug release profile and responses of primary astrocytes were investigated for Dex-loaded and unloaded PSi. A novel strategy to reduce host tissue responses and establish a stable neural interface was proposed for fully implantable neural electrodes via inducing PSi into the microelectrode design and taking advantage of its degradability and drug-loading capability.

2. Materials and methods

First, the methods to form PSi samples and load drugs into the PSi were briefly described. To compare surface properties of samples before and after the drug loading process, surface characterization was then carried out, including SEM, wettability and Fourier transform infrared spectroscopy (FTIR). After further demonstration of drug-loading capability under the fluorescence microscope, biodegradability and drug release profile of the PSi were investigated to explore the drug release mechanism. To evaluate cellular responses to the drug release from the PSi, primary astrocytes were cultured on the surface of samples as the important first step to enable a systematic *in vivo* study in the future.

2.1. Sample preparation

8-in. p-type Si wafers with (1 0 0) crystal orientation and resistivity of 0.002–0.005 Ω-cm purchased from Sumco (Sumco Corp., Japan) were processed via the standard piranha clean procedure to remove the contamination, and then were cut into plates (5 mm × 5 mm, denoted as "Si" hereafter) by dicing saw (DFD 6361, DISCO Corp., Japan). Anodization process was performed to porosify the Si wafer, at a current of 3.5 A, in a 1:1 (v/v) mixture of aqueous hydrofluoric acid (49% HF) and ethanol (99.5%), for 120 min. After being rinsed by distilled water and dried by N_2 flow, the anodized wafer was diced into plates (denoted as "unloaded PSi" hereafter) with the same dimension as Si samples.

Dex solution with a concentration of 5 mg/ml was prepared by dissolving water-soluble Dex (Sigma–Aldrich) into phosphate buffered saline (PBS). Subsequently, PSi samples were incubated into the Dex solution overnight at room temperature to load drugs (denoted as "Dex-loaded PSi" hereafter). Finally, the Dex-loaded PSi samples were rinsed by PBS and distilled water (DIW), and dried in a desiccator.

2.2. Surface characterization

Surface morphology of samples was visualized using field emission scanning electron microscopy (FE-SEM, JSM-6700F, JEOL, USA). Diameter of pores on surfaces of unloaded and Dex-loaded PSi samples was calculated from SEM images using ImageJ software (National Institutes of Health, USA). Wettability of samples was determined by a sessile drop method, using a contact angle goniometer (DSA 100, KRÜSS, Germany) [15]. A drop of distilled water (2 μl) was generated on the surface of samples, and the profile of the drop was immediately recorded by a video camera equipped with the contact angle goniometer. Finally, the contact angle was calculated from the recorded image of the water droplet via an image analysis system in the equipment. Five measurements were conducted for each type of samples at room temperature. Functional groups on surfaces of samples were detected using FTIR (Spectrum BX, Perkin Elmer, USA).

2.3. Drug-loading capability

To demonstrate the drug-loading capability for the PSi under fluorescence microscopy, 1 mg/ml Dex fluorescein (life Technologies) solution in artificial cerebrospinal fluid (ACSF, Harvard Apparatus, Boston, USA) were used to soak PSi samples and PSi backbone developed by our previous studies overnight at room temperature. After being rinsed by ACSF and DIW, and dried in a desiccator, the soaked PSi samples and PSi backbone were observed using a fluorescence microscope (Olympus BX61, Olympus Optical Co., Japan).

2.4. Biodegradability

Biodegradability of unloaded PSi samples was evaluated by an ammonium molybdate colorimetric assay [16]. Briefly, 42 mM ammonium molybdate (Amoly) solution prepared by dissolving ammonium heptamolybdate tetrahydrate salt in DIW was acidified by mixing with 0.3 M HCl in ratio of 1:2 by volume. 1.35 M sodium sulphite solution and 50 mM EDTA solution were prepared by dissolving anhydrous sodium sulphite salt and EDTA disodium salt into DIW, respectively. Unloaded PSi samples were immersed in 1 ml of DIW in a 24-well cell culture plate at 37 °C, and DIW was refreshed every day. 200 μl of DIW containing the degradation product of the PSi was then added into 50 μl Amoly/HCl solution, followed by vortex for 3 s and incubation for 10 min. Subsequently, 25 μl EDTA solution was added into the mixture. After vortex for 3 s and incubation for 5 min, 25 μl sodium sulphite was then blended with the mixed solution. Finally, the solution was aged at room temperature for 1 h and its absorbance was measured using a microplate reader (DTX 800 Series Multimode Detectors, Beckman Coulter, CA, USA) at 600-nm wavelength. All assays were performed in triplicate.

2.5. Drug release studies

In vitro Dex release was studied in PBS at pH 7.4. Dex-loaded PSi samples were soaked in 1 ml of PBS at 37 °C. At defined time intervals, 1 ml of PBS was withdrawn and the released Dex in the solution was determined at 242 nm using UV spectrophotometry (UVmini 1240, Shimadzu Scientific Instruments, USA). 1 ml of fresh PBS was then added back to maintain a constant volume for the incubation medium.

2.6. In vitro biological assessment

2.6.1. Cell culture

Primary rat brain cortex astrocytes purchased from Lonza were cultured in the Astrocyte Growth Medium Bulletkit® (Lonza Walkersville Inc., USA), and incubated at 37 °C in an atmosphere of 5% CO_2 and 95% humidity. After 4 h of culture, the cell medium was refreshed, and then refreshing 50% of cell medium was carried out every 4 days. When the cells were confluent, they were detached by 0.25 (w/v) trypsin–ethylenediaminetetraacetic acid (trypsin–EDTA) (Invitrogen) and counted by an automated cell counter (Luna™, Logos Biosystems, USA).

2.6.2. Cell viability

Viability of primary astrocytes attached on Si, unloaded PSi and Dex-loaded PSi samples was evaluated via a live/dead viability/cytotoxicity kit (Life Technologies Co., USA). Briefly, primary astrocytes were seeded at 2.0×10^4 cells/well onto the surface of samples. Subsequently, the 8-well Lab-Tek® II Chamber Slide™ system (0.7 cm^2/well, Fisher Scientific Inc.) containing samples was incubated at 37 °C in an atmosphere of 5% CO_2 and 95% humidity. After 2 days of cell culture, samples were gently rinsed with PBS, and soaked in 200 ml of PBS containing 2 μM calcein-AM and 2 μM ethidium homodimer-1 for 15 min at 37 °C to stain cells. The living cells were labeled in green due to the enzymatic conversion of the virtually nonfluorescent cell-permeant calcein AM to the intensely fluorescent calcein (excitation/emission, ~495 nm/~515 nm), while dead cells were stained in red as ethidium homodimer-1 entered cells with damaged membranes and produced a bright red fluorescence (excitation/emission, ~495 nm/~635 nm) via binding to nucleic acids. Finally, stained primary astrocytes on surfaces of samples were visualized using the fluorescence microscope. The relative cell number on unloaded and Dex-loaded PSi was determined by normalizing the number of living cells on the samples with those on Si. Additionally, the percentage of activated primary astroctyes on surfaces of samples was calculated and compared. At least seven randomly areas were chosen for the assessment.

2.7. Statistical analyses

All experiments were performed at least three times and all values are expressed as means ± standard errors. The data were compared using one-way analysis of variance (ANOVA) followed by the Tukey's test. $P < 0.05$ was considered to be statistical significance.

3. Results and discussion

3.1. Surface morphology

Fig. 1 shows surface morphology of Si, unloaded PSi, and Dex-loaded PSi samples. The Si surface was quite smooth (Fig. 1a), while disordered and nano featured pores with the diameter of 11.1 ± 7.6 nm were present and homogeneously distributed across the surface of unloaded PSi (Fig. 1b). In principle, PSi is classified in accordance with the pore diameter (D), which can vary from several nanometers to micrometers depending on the processing parameters. Therefore, PSi has been divided into three categories: microporous ($D \leq 2$ nm), mesoporous (2 nm < $D \leq 50$ nm) and microporous ($D > 50$ nm). In this study, on the basis of the pore size (11.1 ± 7.6 nm) mesoporous Si was formed due to the anodization process. After the drug-loading process, however, the diameter of pores on the surface of Dex-loaded PSi reduced to 4.7 ± 2.6 nm (Fig. 1c), indicating that Dex was loaded into the porous structure. Similarly, a significant reduction in the average pore size was reported after a chemical modification of PSi [17]. In addition, no obvious Dex residues were observed, suggesting that the PBS and DIW rinsing process removed most of Dex residues on the surface of samples. Si residue particles resulting from the anodization process were also visualized in SEM images (Fig. 1b and c).

3.2. Cross sectional morphology

Cross sectional morphology of unloaded PSi is shown in Fig. 2. Due to the different electroconductivity, the PSi layer appeared brighter than the Si substrate in SEM images (Fig. 2). The uniform color of the PSi layer in Fig. 2a indicated the homogeneity of the formed PSi layer. Based on the cross sectional morphology of low magnification (Fig. 2a), 70 μm-thick PSi layer was formed on the Si substrate at the current of 3.5 A for 120 min. Hence, the formation rate of the PSi layer is 0.58 μm/min. Fig. 2b illustrates the interface between the PSi layer and the Si substrate at high magnification. A pronounced branching of the pores was clearly visible and the pores were interconnected. Due to a preferential pore propagation along the ⟨1 0 0⟩ crystallographic direction, the coral-like porous structure vertically formed on the Si substrate. The distance between main branches where pores grew ranges from 20 nm to 100 nm. Unlike the PSi formed by stain etching, a relatively sharp interface separated the PSi layer and the Si substrate. Additionally, the cylindrical pores inside the PSi layer can serve as the reservoir to store anti-inflammatory drugs for reduced host tissue responses.

3.3. Wettability

Fig. 3 displays wettability of Si, unloaded PSi, and Dex-loaded PSi samples. Water contact angle of Si samples was 48.5° ± 3.6°, which was in agreement with previous results. Kown et al. suggested that the water contact angle of p-type (1 0 0) Si substrate was 51° [18]. Similar results obtained by Spencer et al. showed that the surface of (1 0 0) oriented B-doped Si wafer was medium hydrophilic (44° ± 3°) [19]. For unloaded PSi, its water contact angle varied in a wide range due to surface instability, porosity, surface topography, the density of Si—H functional groups (surface chemistry), etc. In this study, the water contact angle of unload PSi (34.5° ± 0.5°) was significantly lower than that of Si ($p < 0.05$). The effect of the capillary force on the water contact angle is also responsible for the reduced water contact angle [20]. Since the capillary force is inversely proportional to the pore size, the nano porous structure of the unloaded PSi could generate significant capillary effects that decreased the water contact angle. After the water-soluble drug loading process, a notable decrease in water contact angle was visible for Dex-loaded PSi from 34.5° ± 0.5° to 15.3° ± 1.3° ($p < 0.05$), likely due to the reduced pore size and the incorporation of Dex.

3.4. FTIR spectra

Fig. 4 shows FTIR spectra of surfaces of unloaded PSi and Dex-loaded PSi samples. In terms of the reflection bands corresponding to the chemical functional groups, there was no significant difference in the FTIR spectra between unloaded and Dex-loaded PSi samples, revealing that the remaining Dex residues on the surface of samples were under the minimum detection limit of the FTIR spectrometer. The bands at 1640 and 3600 cm^{-1} were attributed to O—H bending and stretching vibration of absorbed H_2O, respectively [21]. As the FTIR characteristic band of PSi, the band in the range of 2060–2300 cm^{-1} arose from Si—H_x ($x = 1, 2, 3$) stretching modes [22].

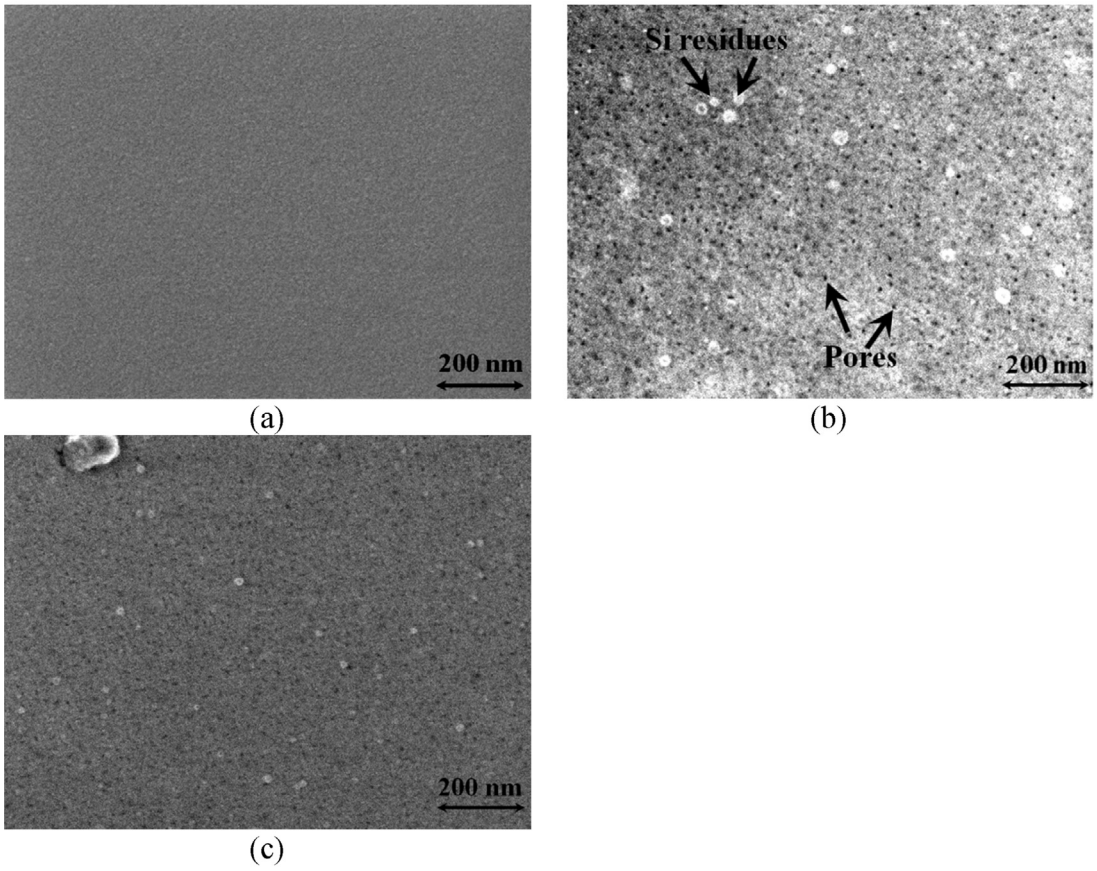

Fig. 1. Surface morphology of (a) Si, (b) unload PSi, and (c) Dex-loaded PSi samples.

3.5. Drug-loading capability

After being soaked into Dex fluorescein solution overnight, rinsed by PBS and DIW, and dried in desiccator, Si and PSi samples (plates), and Si and PSi backbones prepared by our previous study were observed under the fluorescence microscope. Due to no space to store Dex fluorescein and rinse by PBS and DIW, nothing was visualized under the fluorescence microscope for Si samples (Fig. 5a). Similarly, only some small residues of Dex fluorescein attached to the brim of the Si backbone were present, and the shank of the Si backbone did not appear in Fig. 5c (the white dot line indicated the profile of the Si backbone). On the contrary, PSi samples and PSi backbones were stained in green under the fluorescence microscopy for the reason that Dex fluorescein solution flowed through the porous structure and the drugs absorbed onto the inner surface of pores once the solution was evaporated.

3.6. Biodegradability

Fig. 6 illustrates the *in vitro* cumulative degradation curves of Si and unloaded PSi in distilled water for 21 days. Si is not only an essential trace element for normal growth and development of bone and connective tissues, but also reported to be important to vascular health as a dietary supplement [23]. The degradation process of PSi involved two steps: oxidation of the PSi matrix into SiO_2, followed by hydrolysis to nontoxic orthosilicic acid ($Si(OH)_4$),

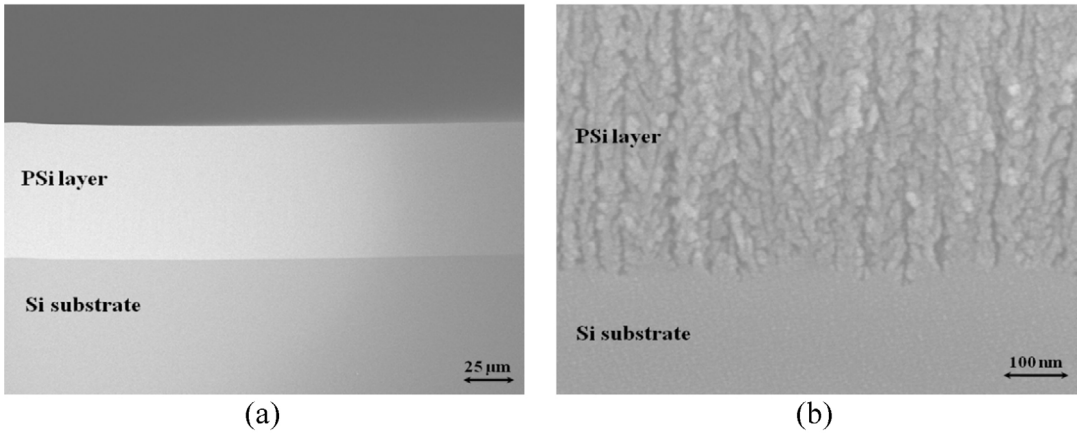

Fig. 2. Cross sectional morphology of unload PSi sample: at (a) low magnification and (b) high magnification.

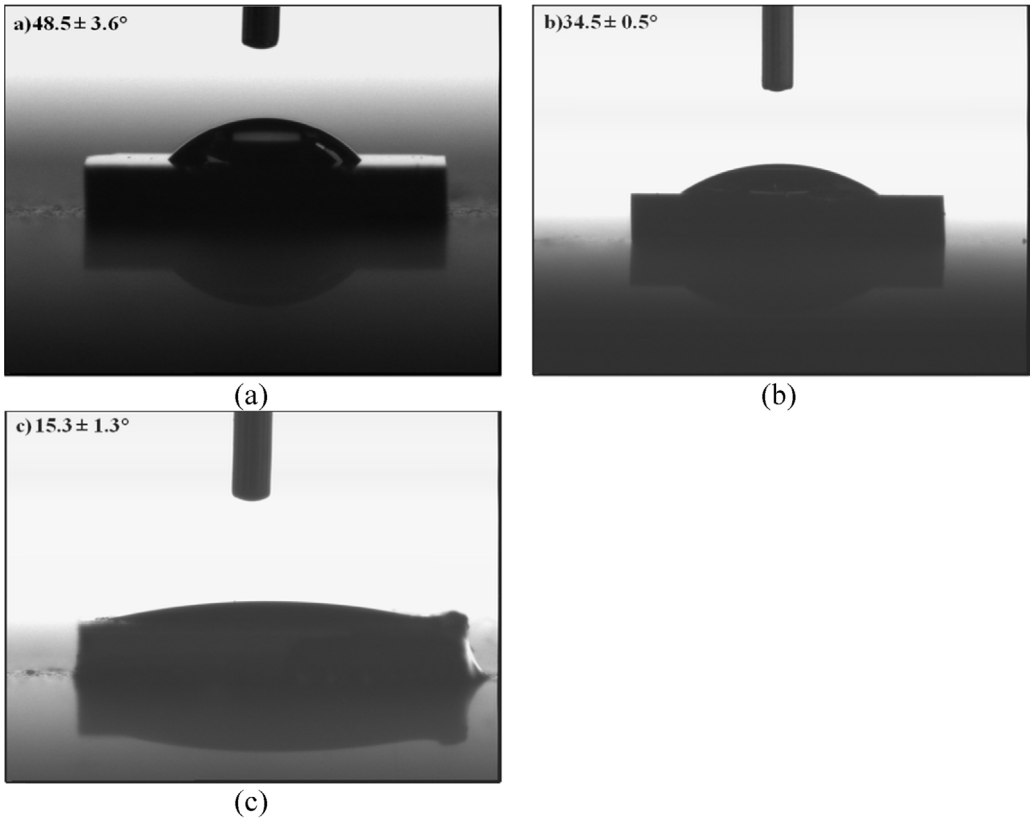

Fig. 3. Water contact angles of (a) Si, (b) Dex-loaded PSi, and (c) Dex-loaded PSi samples.

which was the natural form of Si found in the body and could be excreted by kidneys [24]. To compare the biodegradation behavior, Si samples served as the control. During the biodegradation period, almost no Si ion was detected in the solution for Si samples. On the contrary, 98.1 ± 1.2 μg PSi was degraded and detected in DIW at day 1. For the rest of time points, however, the degradation rate of unload PSi remained almost constant at a level of 17.1 ± 3.8 μg/day, indicating that a sudden degradation occurred at day 1 for unloaded PSi samples. As the cumulative curve did not reach a plateau, unloaded PSi samples did not fully degrade within 3 weeks. Additionally, from day 2 to 21 the relationship between the cumulative amount of degraded PSi and time point was identified by fitting a linear equation ($Y = 92.7 + 17.2 \times X$) to measured data. The biodegradation rate of the raw material is expected to roughly estimate the biodegradation period of the PSi backbone.

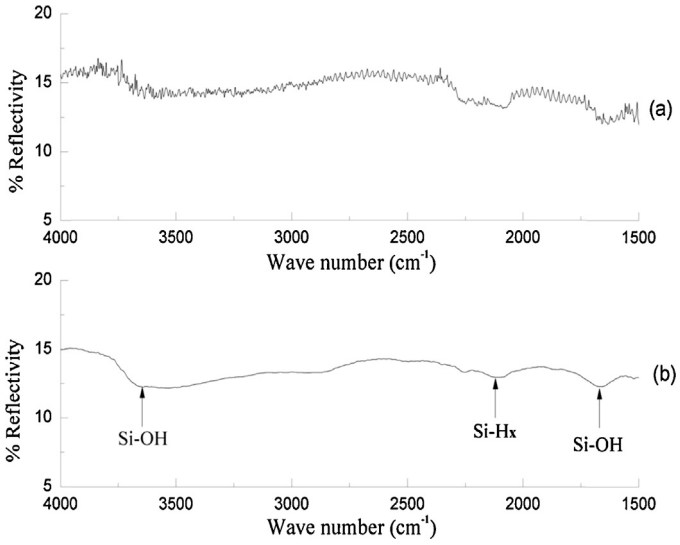

Fig. 4. FTIR spectra of surfaces of (a) unloaded PSi and (b) Dex-loaded PSi samples.

3.7. Drug release

Fig. 7 shows the cumulative drug release profile of Dex-loaded PSi samples in ACSF. The initial burst release was observed in the first 30 h, followed by a sustained release with a slower rate for 102 h. The combined release profile of burst and sustained release was beneficial to the wound treatment which required an initial burst release to provide an immediate relief and a subsequent prolonged release to promote gradual healing. Although the time-scale for the release is hours, the duration of drug release can be extended and near zero-order release can be achieved via surface modification of PSi and subsequent covalent attachment of drugs [24]. In this study, no chemical bonds were formed between Dex and PSi, and Dex physically adsorbed onto the surface or inner surface of PSi diffused into ACSF with the degradation of the PSi. Hence, it was believed that the mechanism of the drug release from PSi was the combination of drug diffusion and PSi degradation [17].

Sustained and controlled drug delivery is one of the most common and effective strategies to minimize host tissue responses to implanted medical devices [25]. Therefore, considerable amount of scientific and technological efforts have been dedicated to integrating drug delivery systems into neural microelectrodes. Polymeric nanoparticles with drug-loading capability have been developed and assembled on the surface of dummy silicon dioxide neural probe, in order to realize controlled, sustained and simultaneous release of multiple biomoleculars or drugs [26]. Although the drug release sustained for more than two weeks, the electrical properties of functional microelectrodes might be deteriorated due to

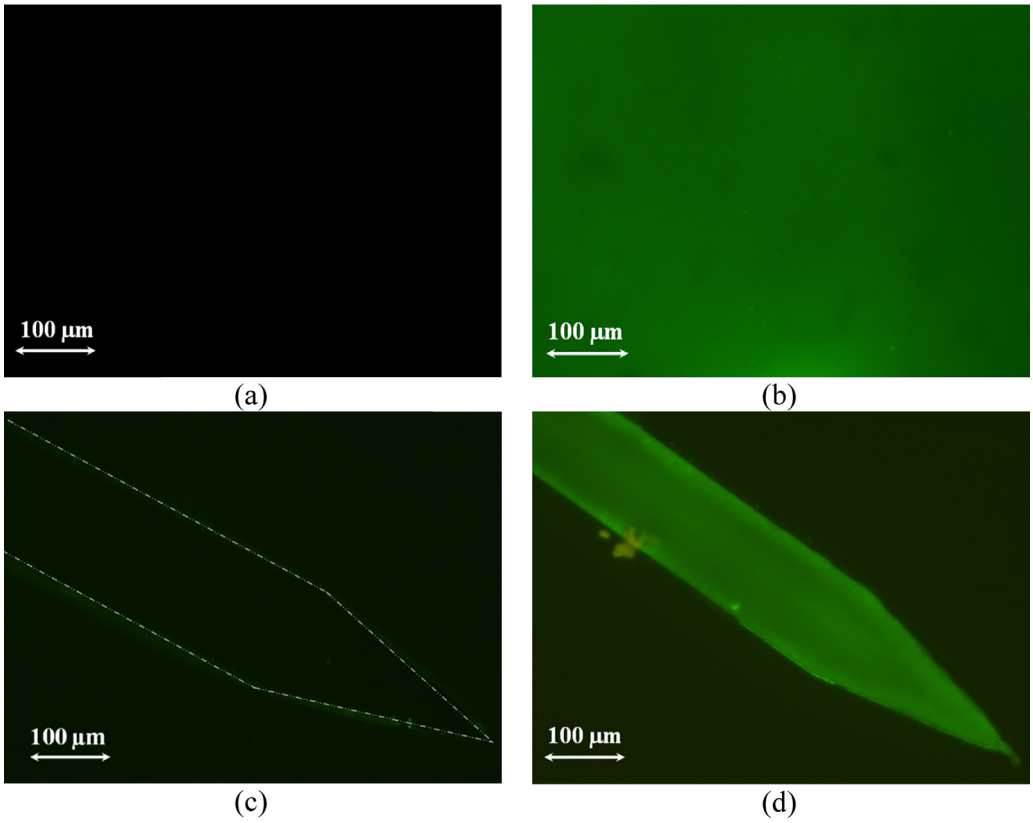

Fig. 5. Fluorescence images of surfaces of (a) Si sample, (b) PSi sample, (c) Si backbone, and (d) PSi backbone after incubation in 1 mg/ml Dex fluorescein solution overnight (the white dot line indicated the profile of the Si backbone). (For interpretation of the references to color in the text, the reader is referred to the web version of the article.)

the attachment of the nonconductive polymeric particles on the recording sites. Moreover, flexible microelectrode with microfluidic channels was designed to deliver drugs to cortical tissues and reduce host tissue responses [27]. But cumbersome pumping system is usually required to deliver drugs via microfludic channels, and hence can give rise to additional tissue damage and potential infection. In our study, PSi serves not only as the backbone to strength the microelectrode for implantation, but also as the reservoir to store and release drugs to surrounding tissues. With the degradation of PSi in cortical tissues, the drugs are released to suppress host tissue responses, the dimension of the microelectrode is gradually diminished to facilitate the tissue healing process, and the mechanical properties of the microelectrode (the remaining flexible polymer part) eventually match with those of cortical tissue to reduce the post-implantation injury. In future studies, surface modification of the PSi backbone and covalently attaching drugs onto its surface will be investigated to enhance its biocompatibility and elongate the duration of drug delivery.

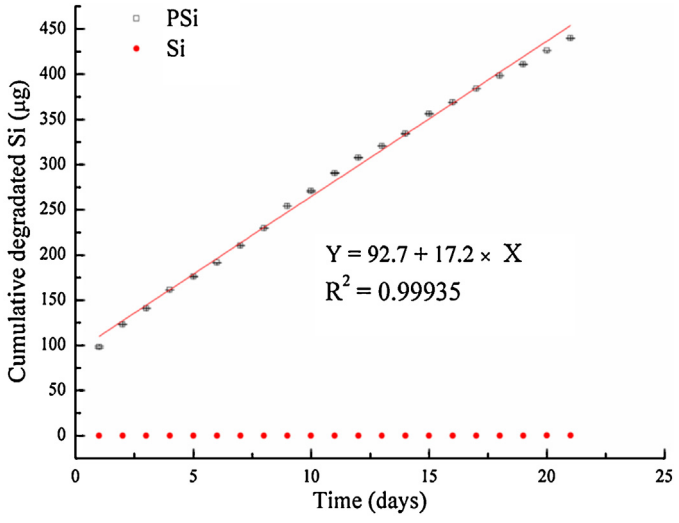

Fig. 6. Cumulative degradation curve of Si and unloaded PSi samples in distilled water.

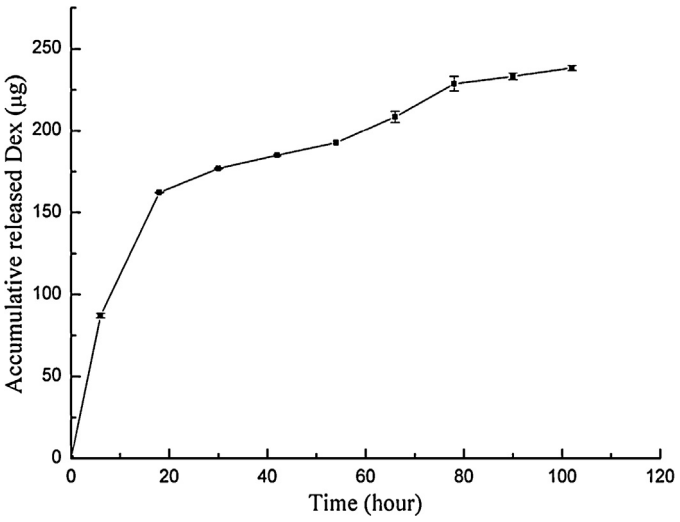

Fig. 7. Cumulative drug release profile of Dex-loaded PSi samples in ACSF.

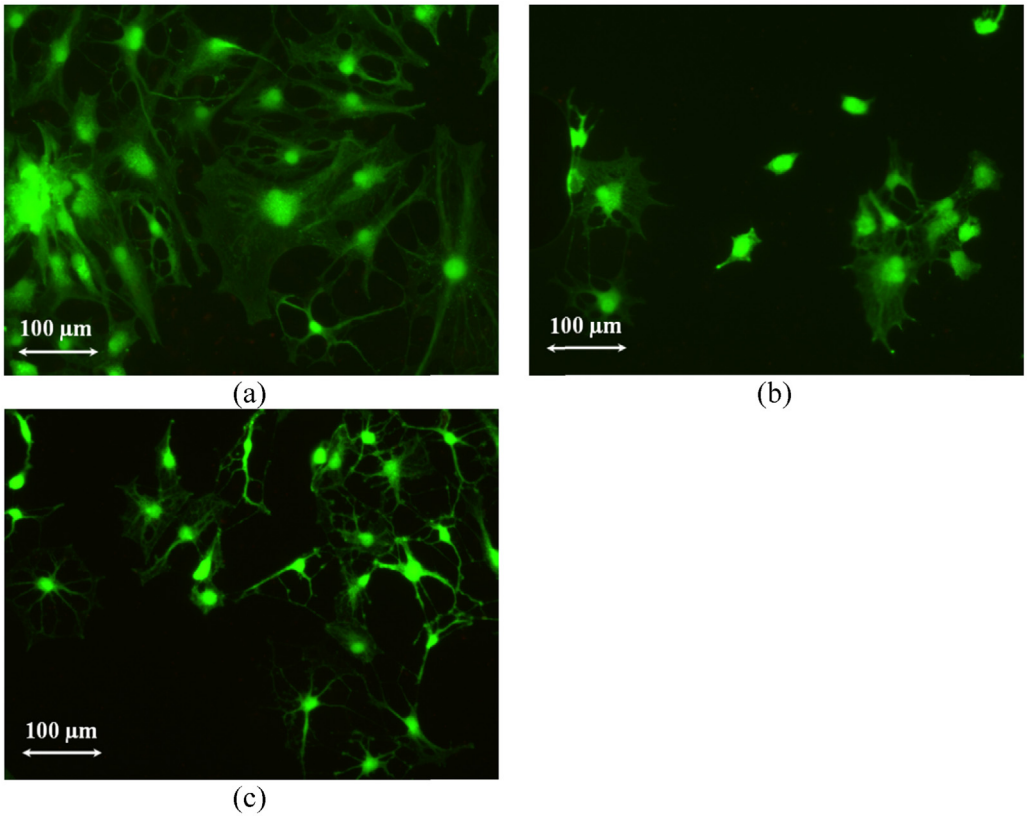

Fig. 8. After 2 days of cell culture, representative morphology of primary astrocytes on (a) Si, (b) unloaded PSi and (c) Dex-loaded PSi samples.

3.8. Cell viability

Morphology of primary astrocytes seeded onto surfaces of Si, unloaded PSi, and Dex-loaded PSi samples was shown in Fig. 8. Primary astrocytes were identified by stellate shape in terms of morphology. But reactive astrocytes were characterized by irregular nucleus, enlarged cell bodies occasionally with multiple hypertrophic processes, increased matrix production, upregulation of proliferation, etc. [28,29]. For Si, unloaded PSi, and Dex-loaded PSi samples, few dead primary astrocytes were visualized on their surfaces. But primary astrocytes preferred to attach to the surface of Si in comparison with unloaded or Dex-loaded PSi, and the number of cells present on the surface of unloaded PSi was less than that of Dex-loaded PSi ($p < 0.05$). For unloaded and loaded PSi, relative cell numbers on their surfaces were 51.7% ± 6.5% and 77.9% ± 14.3% of those on Si surface, respectively. Hence, on the basis of the fluorescence images recorded from randomly chosen areas, the relative number of primary astrocytes adherent on the surface of samples was counted, and increased in the order of unloaded PSi < Dex-loaded PSi < Si (Fig. 9a).

The reduced astrocyte attachment on unloaded PSi surface was in agreement with previous *in vitro* investigation. Study conducted by Moxon et al. showed the concurring results that the astrocyte density on bare PSi was around half of that on Si [30]. The low cell

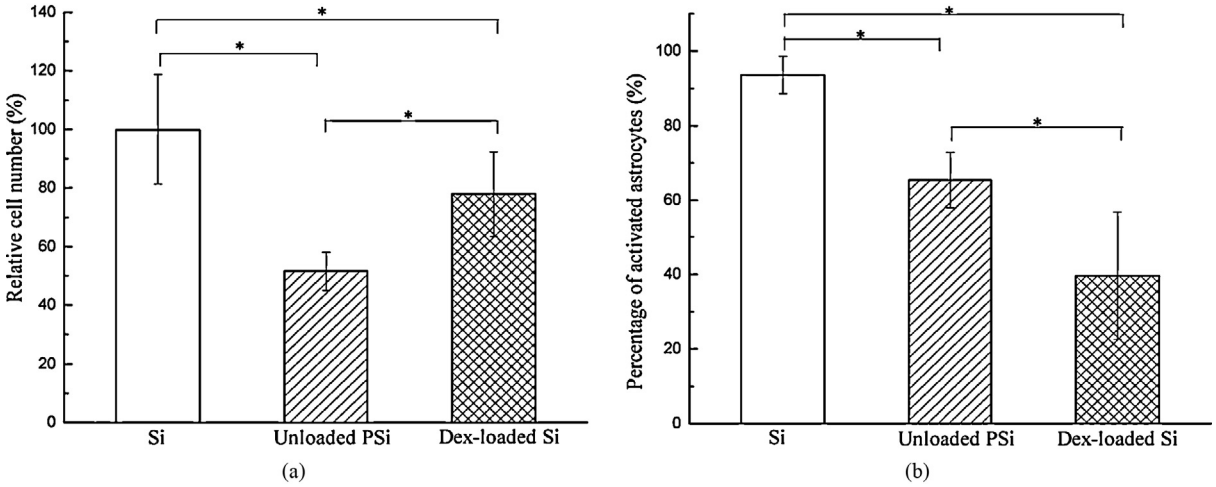

Fig. 9. After 2 days of cell culture, (a) relative cell number on Si, unloaded PSi and Dex-loaded PSi samples; (b) the percentage of activated primary astrocytes on Si, unloaded PSi and Dex-loaded PSi samples. An asterisk indicates statistical significance ($p < 0.05$).

attachment to bare PSi surface might be attributed to the unstable SiH_x ($x = 1$, 2 and 3) functional groups, arising from anodization process (HF solution). Many surface modification methods, such as thermal oxidation, protein or biomolecular coatings, amino silanisation, were investigated to stabilize PSi surface and enhance cell attachment [31–33]. In this research, the unstable SiH_x functional groups might decrease after the drug-loading process, and astrocytes were hence prone to attach to the surface of Dex-loaded PSi samples.

Although more primary astrocytes exhibited on the surface of Dex-loaded PSi than unloaded PSi, only 39.7% ± 17.1% of them possessed the morphological feature of activated astrocytes after 2 days of cell culture (Fig. 9b). On the contrary, most of primary astrocytes on the surfaces of Si (93.5% ± 5%) and unloaded PSi (65.3% ± 7.4%) were activated, as evidenced by florescence images (Fig. 8). Therefore, Dex-loaded PSi not only moderately prevented astrocyte adhesion, but also effectively suppressed the activation of primary astrocytes due to the drug release. More importantly, Dex-loaded PSi did not show the cytotoxicity due to the observation of few dead cells.

Cellular responses to the implanted neural microelectrode at early time points are critical in determining the stable neural interface. Szarowski et al. reported that after 1 day of microelectrode insertion activated astrocytes was observed at the region 100–200 μm away from the implantation site [34]. A gradual increase of astrocyte activation was then found through 1 and 2 weeks, until a dense encapsulation layer formed at 4 weeks. Subsequently, the fibrous sheath remained constant and fewer activated astrocytes were present around the implant. As activated astrocytes are the major component of the fibrous encapsulation tissue surrounding microelectrodes, it was thought that astrocyte activation at early time points played a critical role in the formation of the encapsulation tissue which progressively isolated implanted microelectrodes and extended the distance between recording sites and neurons [6]. Therefore, it might be an effective method to maintain recording stability via the suppression of astrocyte activation at early time points. By means of loading drugs into the PSi backbone, the proposed PSi-polymer hybrid microelectrode has potential to further reduce the host tissue responses *in vivo* and the neural signal recording might remain stable.

4. Conclusions

As a critical component of the microelectrode to record brain activities, uniform PSi layer 70 μm in thickness was formed on Si substrate via the anodization process. The mean growth rate and pore size of the PSi layer was 0.58 μm/min and 11.1 ± 7.6 nm, respectively. For the stable neural interface, Dex was loaded into the PSi by the incubation with the drug solution overnight. After the drug loading process, both the pore size and water contact angle decreased, and fluorescence images demonstrated the drug loading capability of the PSi. For the PSi degradation in distilled water, a sudden degradation took place at day 1, while the degradation rate remained almost constant at a level of 17.1 ± 3.8 μg/day for the rest of time points up to day 21. Furthermore, the drug release profile of the Dex-loaded PSi was characterized by a combination of an initial burst release and subsequent sustained release. Although more astrocytes attached to the surface of Dex-loaded PSi than unloaded PSi, the released Dex could remarkably reduce the activation of astrocytes. Hence, it might be an effective strategy to minimize the host tissue responses and establish the stable neural interface via integrating drug loaded PSi into microelectrodes.

Acknowledgements

The authors gratefully acknowledge staffs in the Bioelectronics Lab, Institute of Microelectronics for their generous help and valuable suggestions. This work was supported by the Science and Engineering Research Council of Agency for Science, Technology and Research (A*STAR) under Grant 1021710159, and also by Basic Science Research Program through the National Research Foundation of Korea (NRF) funded by the Ministry of Science, ICT & Future Planning (NRF-2013R1A1A1012616).

References

[1] M.A.L. Nicolelis, Actions from thoughts, Nature 409 (2001) 403–407.
[2] A.B. Schwartz, X.T. Cui, D.J. Weber, D.W. Moran, Brain-controlled interfaces: movement restoration with neural prosthetics, Neuron 52 (2006) 205–220.
[3] J.C. Williams, R.L. Rennaker, D.R. Kipke, Long-term neural recording characteristics of wire microelectrode arrays implanted in cerebral cortex, Brain Research Protocols 4 (1999) 303–313.
[4] L.R. Hocherg, M.D. Serruya, G.M. Friehs, J.A. Mukand, M. Saleh, A.H. Caplan, A. Branner, D. Chen, R.D. Penn, J.P. Donoghue, Neuronal ensemble control of prosthetic devices by a human with tetraplegia, Nature 442 (2006) 164–171.
[5] J.D. Simeral, S.P. Kim, M.J. Black, J.P. Donoghue, L.R. Hochberg, Neural control of cursor trajectory and click by a human with tetraplegia 1000 days after implant of an intracortical microelectrode array, Journal of Neural Engineering 8 (2011) 025027.
[6] V.S. Polikov, P.A. Tresco, W.M. Reichert, Response of brain tissue to chronically implanted neural electrodes, Journal of Neuroscience Methods 148 (2005) 1–18.
[7] E. Azemi, C.F. Lagenaur, X.T. Cui, The surface immobilization of the neural adhesion molecule L1 on neural probes and its effect on neuronal density and gliosis at the probe/tissue interface, Biomaterials 32 (2011) 681–692.
[8] T. Sun, W.T. Park, M.Y. Cheng, J.Z. An, R.F. Xue, K.L. Tan, M. Je, Implantable polyimide cable for multichannel high-data-rate neural recording Microsystems, IEEE Transactions on Biomedical Engineering 59 (2012) 390–399.
[9] F. Johansson, L. Wallman, N. Danielsen, J. Schouenborg, M. Kanie, Porous silicon as a potential electrode material in a nerve repair setting: tissue reactions, Acta Biomaterialia 5 (2009) 2230–2237.
[10] A. Misra, P. Kondaveeti, J. Nissanov, K. Barbee, P. Shewokis, L. Rioux, K.A. Moxon, Preventing neuronal damage and inflammation in vivo during cortical microelectrode implantation through the use of Poloxamer P-188, Journal of Neural Engineering 10 (2013) 016011.
[11] T. Sun, W.T. Park, G.K. Tay, M. Je, A study on biocompatibility for a microfabricated biodegradable porous silicon probe, in: Proceeding of 6th Asia-Pacific Conference on Transducers and Micro/Nano Technologies (APCOT 2012), Nanjing, China, 2012.
[12] L. Spataro, J. Dilgen, S. Retterer, A.J. Spence, M. Isaacson, J.N. Turner, W. Shain, Dexamethasone treatment reduces astroglia responses to inserted neuroprosthetic devices in rat neocortex, Experimental Neurology 194 (2005) 289–300.
[13] Y. Zhong, R.V. Bellamkonda, Dexamethasone-coated neural probes elicit attenuated inflammatory response and neuronal loss compared to uncoated neural probes, Brain Research 1148 (2007) 15–27.
[14] D.H. Kim, D.C. Martin, Sustained release of dexamethasone from hydrophilic matrices using PLGA nanoparticles for neural drug delivery, Biomaterials 27 (2006) 3031–3037.
[15] T. Sun, W.C. Lee, M. Wang, A comparative study of apatite coating and apatite/collagen composite coating fabricated on NiTi shape memory alloy through electrochemical deposition, Materials Letters 65 (2011) 2575–2577.
[16] T. Sun, J.Z. An, W.T. Park, M. Je, Effect of solution aging time on stability of colorimetric assay for degradation rate evaluation of porous Si in artificial cerebrospinal fluid, Advanced Materials Research 651 (2013) 306–311.
[17] A. Tzur-Balter, A. Gilert, N. Massad-Ivanir, E. Segal, Engineering porous silicon nanostructures as tunable carriers for mitoxantrone dihydrochloride, Acta Biomaterialia 9 (2013) 6208–6217.
[18] Y.B. Kwon, B.M. Weon, K.H. Won, J.H. He, Y. Hwu, G. Margaritondo, X-ray-induced changes in wettability, Langmuir 25 (2009) 1927–1929.
[19] S.J. Spencer, G.T. Andrews, C.G. Deacon, Contact angle of ethanol–water solutions on crystalline and mesoporous silicon, Semiconductor Science and Technology 28 (2013) 055011.
[20] R.A. Fleming, M. Zou, Silica nanoparticle-based films on titanium substrates with long-term superhydrophilic and superhydrophobic stability, Applied Surface Science 280 (2013) 820–827.
[21] T. Sun, L. Wang, M. Wang, (Ti, O)/Ti and (Ti, O, N)/Ti composite coatings fabricated via PIIID for the medical application of NiTi shape memory alloy, Journal of Biomedical Materials Research Part B: Applied Biomaterials 968 (2011) 249–260.
[22] Z.C. Feng, A.T.S. Wee, K.L. Tan, Surface and optical analyses of porous silicon membranes, Journal of Physics D: Applied Physics 27 (1994) 1968.
[23] R. Jugdaohsingh, S.H.C. Anderson, K.L. Tucker, H. Elliott, D.P. Kiel, R.P.H. Thompson, Dietary silicon intake and absorption, American Journal of Clinical Nutrition 75 (2002) 887–893.

[24] E.C. Wu, J.S. Andrew, L. Cheng, W.R. Freeman, L. Pearson, M.J. Sailor, Real-time monitoring of sustained drug release using the optical properties of porous silicon photonic crystal particles, Biomaterials 32 (2011) 1957–1966.
[25] S. Franz, S. Rammelt, D. Scharnweber, J.C. Simon, Immune responses to implants—a review of the implications for the design of immunomodulatory biomaterials, Biomaterials 32 (2011) 6692–6709.
[26] C.T. Lo, P.R. Van Tassel, W.M. Saltzman, Poly(lactide-co-glycolide) nanoparticle assembly for highly efficient delivery of potent therapeutic agents from medical devices, Biomaterials 31 (2010) 3631–3642.
[27] S. Takeuchi, D. Ziegler, Y. Yoshida, K. Mabuchi, T. Suzuki, Parylene flexible neural probes integrated with microfluidic channels, Lab on a Chip 5 (2005) 519–523.
[28] F. Du, Li Zhu, Z. Qian, X.M. Wu, W.H. Yung, W.Y. Xu, Y. Ke, Expression of bystin in reactive astrocytes induced by ischemia/reperfusion and chemical hypoxia in vitro, Biochimica et Biophysica Acta 1782 (2008) 658–663.
[29] K. Oki, N. Kaneko, H. Kanki, T. Imai, N. Suzuki, K. Sawamoto, H. Okano, Musashi1 as a marker of reactive astrocytes after transient focal brain ischemia, Neuroscience Research 66 (2010) 390–395.
[30] K.A. Moxon, N.M. Kalkhoran, M. Markert, M.A. Sambito, Nanostructured surface modification of ceramic-based microelectrodes to enhance biocompatibility for a direct brain–machine interface, IEEE Transactions on Biomedical Engineering 51 (2004) 881–889.
[31] J. Charrier, V. Alaiwan, P. Pirasteh, A. Najar, M. Gadonna, Influence of experimental parameters on physical properties of porous silicon and oxidized porous silicon layers, Applied Surface Science 253 (2007) 8632–8636.
[32] M.J. Sweetman, F.J. Harding, S.D. Graney, N.H. Voelcker, Effect of oligoethylene glycol moieties in porous silicon surface functionalisation on protein adsorption and cell attachment, Applied Surface Science 257 (2011) 6768–6774.
[33] S.P. Low, K.A. Williams, L.T. Canham, N.H. Voelcker, Evaluation of mammalian cell adhesion on surface-modified porous silicon, Biomaterials 27 (2006) 4538–4546.
[34] D.H. Szarowski, M.D. Andersen, S. Retterer, A.J. Spence, M. Isaacson, H.G. Craighead, J.N. Turner, W. Shain, Brain responses to micro-machined silicon devices, Brain Research 983 (2003) 23–35.